Multiple-Frequency EPR Spectra of Two Aqueous Gd^{3+} Polyamino Polypyridine Carboxylate Complexes: A Study of High Field Effects

Alain Borel,*,† Sabrina Laus,† Andrzej Ozarowski,‡ Christelle Gateau,§ Aline Nonat,§ Marinella Mazzanti,§ and Lothar Helm†

Laboratoire de Chimie Inorganique et Bioinorganique, Ecole Polytechnique Fédérale de Lausanne, CH-1015 Lausanne, Switzerland, National High Magnetic Field Laboratory, Florida State University, Tallahassee, Florida 32310, and Laboratoire de Reconnaissance Ionique and Chimie de Coordination, Service de Chimie Inorganique et Biologique (UMR-E 3 CEA-UJF), Département de Recherche Fondamentale sur la Matière Condensée, SCIB/DRFMC/DSM CEA-Grenoble, 17 rue des Martyrs, 38054 Grenoble, Cedex 09, France

Received: October 22, 2006; In Final Form: April 11, 2007

In the search for highly efficient magnetic resonance imaging contrast agents, polyamino polypyridine carboxylate complexes of Gd^{3+} have shown unusual properties with both very rapid and very slow electron spin relaxation in solution observed by electron paramagnetic resonance. Since the relationship between the molecular structure and the electron spin properties remains quite obscure at this point, detailed studies of such complexes may offer useful clues for the design of Gd^{3+} compounds with tailored electronic features. Furthermore, the availability of very high-frequency EPR spectrometers based on quasi-optical components provides us with an opportunity to test the existing relaxation theories at increasingly high magnetic fields and observation frequencies. We present a detailed EPR study of two gadolinium polyamino polypyridine carboxylate complexes, $[Gd(tpaen)]^-$ and $[Gd(bpatcn)(H_2O)]$, in liquid aqueous solutions at multiple temperatures and frequencies between 9.5 and 325 GHz. We analyze the results using the model of random zero-field splitting modulations through Brownian rotation and molecular deformations. We consider the effect of concentration on the line width, as well as the possible existence of an additional *g*-tensor modulation relaxation mechanism and its possible impact on future experiments. We use ^{17}O NMR to characterize the water exchange rate on $[Gd(bpatcn)(H_2O)]$ and find it to be slow ($\sim 0.6 \times 10^6$ s^{-1}).

Introduction

Gd^{3+} complexes with multidentate ligands are routinely used in medicine as contrast agents for magnetic resonance imaging (MRI). They accelerate the magnetic relaxation of the water protons due to random modulations of the interaction with the seven unpaired electrons of the Gd^{3+} center. This effect is usually quantified by the *relaxivity*, namely, the longitudinal relaxation rate enhancement observed in the presence of a unit concentration (1 mM) of the paramagnetic agent. Of course, understanding the molecular origins of this enhancement is the key to developing new and improved contrast agents. Therefore, the magnetic properties of these complexes have been probed using a number of techniques, such as ^1H NMR (in the form of nuclear magnetic relaxation dispersion − NMRD), ^{17}O NMR,[1,2] and electron paramagnetic resonance (EPR).[3−7]

Due to the toxicity of the $[Gd(H_2O)_8]^{3+}$ aqua ion, it is necessary to embed the Gd^{3+} ion in highly stable chelates for the development of potential contrast agents. The ligands are generally polyaminocarboxylates, the basic example of which is the well-known hexadentate $edta^{4-}$ (ethylene diamine tetracarboxylate). However, a higher denticity is usually necessary to achieve sufficient stability. The commercial contrast agent ligands ($dota^{4-}$, $dtpa^{5-}$, dtpa-bma^{3-}, hp-$do3a^{3-}$) occupy eight coordination sites around the metal, leaving only one available position for a water molecule. This reduced hydration number has an obvious negative impact on relaxivity, as the chemical exchange of water molecules bound to the paramagnetic center is an efficient way to enhance the overall water proton relaxation rate. It also affects the electron spin relaxation rates by changing the zero-field splitting (ZFS) due to the different ligand field. A major trend of research in recent years has been to increase the relaxivity through an increase in molecular weight[8−11] or binding to macromolecules,[12−14] or an acceleration of water exchange.[8,15] Although less attention has been devoted to this aspect of relaxivity, it is worthwhile to investigate alternative ligand designs that could optimize the electron spin relaxation properties.

After fairly high relaxivities have been observed for two complexes of tripodal ligands with pyridinecarboxylate arms,[16,17] the heptadentate $tpaa^{3-}$ (6,6′,6″-[nitrilotris(methylene)]tris[2-pyridinecarboxylate]) and the nonadentate $tpatcn^{3-}$ (6,6′,6″-[(hexahydro-1*H*-1,4,7-triazonine-1,4,7-triyl)tris(methylene)]tris-[2-pyridinecarboxylate]), it was suggested that very slow electron spin relaxation might occur in those complexes.[18] This finding was later confirmed by EPR.[19] The typical X-band EPR (9−9.5 GHz) spectrum of a Gd^{3+} chelate in solution is a broad, roughly Lorentzian line. The peak-to-peak width, related to the transverse relaxation rates, is usually between 50 and 1000 G, depending on the molecule and the temperature. At higher EPR frequencies, the lines become sharper. In good agreement with

* Corresponding author: Alain Borel, Institut des sciences et ingénierie chimiques, EPFL-SB-SCGC-BCH, CH-1015 Lausanne, Switzerland; Fax: +41 21 693 9805; e-mail: alain.borel@epfl.ch.
† Ecole Polytechnique Fédérale de Lausanne.
‡ Florida State University.
§ SCIB/DRFMC/DSM CEA.

10.1021/jp066921z CCC: $37.00
Published on Web 06/01/2007

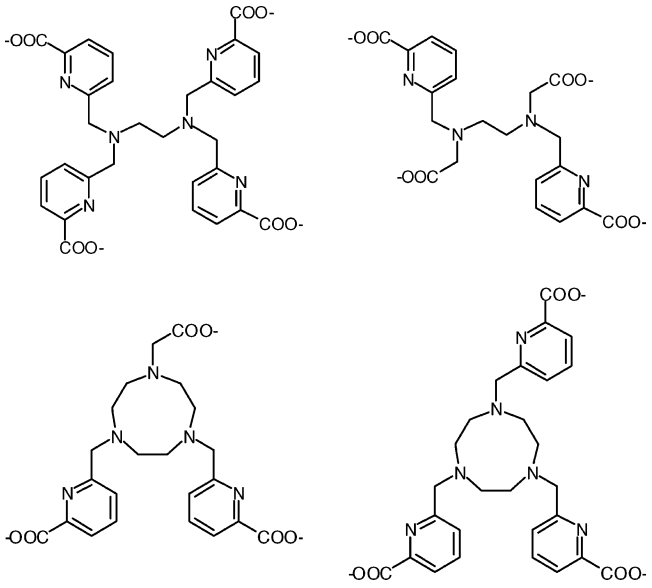

Figure 1. The $tpaen^{4-}$ (upper left), $bpeda^{4-}$ (upper right), $bpatcn^{3-}$ (lower left), and $tpatcn^{3-}$ (lower right) ligands.

the NMRD profile, the apparent peak-to-peak width of [Gd(tpatcn)] was in the 10−20 G region at X-band and 8−12 G at W-band (∼94 GHz). The lines were actually so sharp that the spectrum of a ^{157}Gd-enriched complex (natural abundance 15.65%, $I = 3/2$) allowed an unambiguous determination of the hyperfine coupling constant with the metal nucleus. The electron spin relaxation of this complex was also measured by NMR, yielding the longest effective electron relaxation time at zero field reported to date (1500 ps, compared to ∼650 ps for $[Gd(dota)(H_2O)]^-$).[20] It was suggested that the nitrogen-rich coordination polyhedron of the Gd^{3+} center in this complex (six out of nine coordination sites) might be the origin of a weaker ligand field acting on the f orbitals, leading to a rather small ZFS and consequently to a slow electron spin relaxation in solution. However, [Gd(tpatcn)] is not suitable as a potential MRI contrast agent, because no exchangeable water molecule is bound to the metal ion, which seriously limits its relaxivity.

A later study on another polyamino polypyridine carboxylate complex, $[Gd(bpeda)(H_2O)]^-$ ($bpeda^{4-}$ = 6,6′,6″,6‴-[1,2-ethanediylbis[nitrilobis(methylene)]]tetrakis[2-pyridinecarboxylate]), showed that the pyridine carboxylate moiety itself cannot be the single origin of the slow electron spin relaxation observed for [Gd(tpatcn)].[21] The EPR lines of solutions of $[Gd(bpeda)(H_2O)]^-$ were very broad (peak-to-peak width 800−1200 G at X-band, 90−110 G at Q-band). However, the replacement of carboxylate groups with pyridine carboxylates remains an attractive strategy for the design of nitrogen-rich ligands, with possible luminescence applications as well.[22] In order to fully assess the potential of that ligand type, further investigation was needed. In this article, we use EPR over a very broad frequency range (9.5−325 GHz) to probe the electron spin relaxation of two recently prepared polyamino polypyridine carboxylate complexes,[22,23] $[Gd(tpaen)]^-$ and $[Gd(bpatcn)(H_2O)]$ ($tpaen^{4-}$ = 6-[[(2-carboxyethyl)[2-[(carboxymethyl)[(6-carboxy-2-pyridinyl)methyl]amino]ethyl]amino]methyl]- 2-pyridinecarboxylate; $bpatcn^{3-}$ = 4,7-bis[(6-carboxy-2-pyridinyl)methyl]octahydro-1*H*-1,4,7-triazonine-1-acetate; see Figure 1). The former is a ten-coordinate analog of $[Gd(bpeda)(H_2O)]^-$ with more coordination sites occupied by nitrogen atoms, and the latter sacrifices one pyridine carboxylate arm compared to [Gd(tpatcn)] in order to accommodate one inner-sphere water molecule. Previous NMR studies of the $[Gd(bpatcn)(H_2O)]$ complex showed a shorter effective electron spin relaxation time at zero field with respect to the more symmetric [Gd(tpatcn)]. However, more favorable electron relaxation properties were foreseen as compared to $[Gd(bpeda)(H_2O)]^-$ presenting the same type of donor atoms but included in a different architecture. Finally, we also used ^{17}O NMR to determine the chemical exchange rate of that water molecule, an important factor in the design of high-relaxivity contrast agents.

Experimental Section

EPR Spectroscopy. An 8.1 mM $[Gd(bpatcn)(H_2O)]$ solution was prepared in situ by reacting $GdCl_3$ with the protonated ligand in water and subsequently adjusting the pH at ∼6 with KOH. Dilutions with bidistilled water yielded solutions with concentrations of 2.2 and 0.49 mM. The same procedure was followed with $[Gd(tpaen)]^-$ for a final concentrations of 13.2 mM. Solutions with $[Gd^{3+}] = 3.4$ and 0.78 mM were obtained by dilution.

EPR spectra at X- and Q-band (9.4 and 34 GHz, respectively) were recorded on a Bruker Elexsys E500 system. The microwave frequency was measured using a frequency counter embedded in the standard microwave bridge (X-band) or an external Hewlett-Packard 5353B frequency counter (Q-band). The temperature was varied between 274 and 340 K using boiling nitrogen flowing over a thermoresistor, and measured with a standard substitution technique.[24] W-band (94.5 GHz) spectra were recorded on a Bruker Elexsys E580 spectrometer.[25] Spectra at very high frequencies (VHF) were acquired on a quasi-optical spectrometer developed at the National High Magnetic Field Laboratory (Tallahassee, FL) operating in reflection mode. The instrument is similar to that of Smith,[26] with a 108.5 GHz Gunn diode as a microwave source and frequency multipliers allowing for 217 and 325 GHz.

The peak-to-peak widths ΔH_{pp} and central fields B_0 were determined by fitting the digitally recorded spectra to Lorentzian derivatives, with simultaneous baseline and phase correction.[27] At W-band and higher frequencies, we took into account the hyperfine coupling with the NMR-active Gd isotopes in the line shape analysis by using a hyperfine coupling constant fixed to the value observed for [Gd(tpatcn)] (4.34 and 5.67 G for ^{155}Gd and ^{157}Gd, respectively).[19] The X-, Q-, and W-band line widths and positions were then analyzed within the framework of the Rast model.[7,28,29] Indeed, using only the reduced values ΔH_{pp} and B_0 instead of the full line shape makes it easier to account for new factors such as hyperfine coupling, concentration, or instrumental effects, unrelated with the originally proposed relaxation mechanism. The Rast model assumes that the electron spin relaxation is determined by the so-called static or average ZFS, which is modulated by molecular tumbling, and by the transient ZFS, which is rapidly modulated by random distortions of the complex. Here, we limited the static and transient ZFS to second-order, although fourth- and sixth-order terms are also possible for a spin $S = {}^7/_2$. The least-squares fit procedure yields the following parameters: the static ZFS magnitude parameter a_2, the rotational correlation time at room temperature $\tau_R^{298} = 1/(6D_R)$ and activation energy E_R, the transient ZFS magnitude a_{2T}, the associated correlation time τ_v^{298} and activation energy E_v, plus the natural isotropic g-factor in the absence of relaxation. To reduce the number of adjustable parameters, the rotational correlation time was fixed to the value obtained from the Stokes equation based on the Connolly volume[30] for simple models of both complexes (100 ps for $[Gd(tpaen)]^-$, 120 ps for $[Gd(bpatcn)(H_2O)]$). Furthermore, as the apparent g-factor $g^{app} = (h\nu/\mu_B B_0)$ converges toward its natural value with increasing

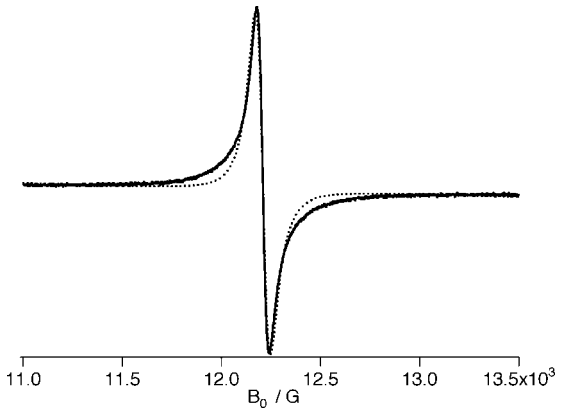

Figure 2. Q-band (33.9655 GHz) spectrum of $[Gd(tpaen)]^-$ at 321.6 K (full line) and the best-fitting single Lorenzian derivative (dotted line).

frequency (as noted by Clarkson et al.[5] using a transient-only ZFS relaxation mechanism) due to the $1/\nu$ decay of the imaginary part of the spectral densities causing the dynamic frequency shift, the natural *g*-factor was fixed to its approximate value at the highest available EPR frequency (1.9924 at 325 GHz). In a second phase, the VHFEPR data were added, and the same analysis was performed over all available measurements.

^{17}O NMR Spectroscopy. A $[Gd(bpatcn)(H_2O)]$ sample was prepared by mixing equimolar amounts of $GdCl_3$ and ligand solutions. An excess (20%) of ligand was used, and the pH was adjusted by adding known amounts of HCl or KOH. The absence of free metal was checked by a xylenol orange test at pH ~6.[31] The reference sample (acidified water) and the Gd^{3+} complexes were enriched to 1% with ^{17}O-enriched water (Isotrade GmbH) to improve sensitivity. The concentration of the Gd^{3+} ion was checked by ICP-AES. The compositions of the samples were $[Gd^{3+}] = 0.03057$ mol kg^{-1} (pH = 6.02).

Transverse and longitudinal ^{17}O relaxation rates and chemical shifts were measured for temperatures between 274 and 366 K. The data were recorded on a Bruker DRX (9.4 T, 54.2 MHz). A Bruker VT 3000 temperature control unit was used to maintain a constant temperature, which was measured by the substitution technique.[24] The samples were sealed in glass spheres, fitting into 10 mm NMR tubes, in order to eliminate susceptibility corrections to the chemical shifts.[32] Longitudinal relaxation rates, $1/T_1$, were obtained by the inversion recovery method,[33] and transverse relaxation rates, $1/T_2$, were measured by the Carr-Purcell-Meiboom-Gill spin echo technique.[34]

Results

The EPR spectra of both complexes are quite similar. At X- and Q-band, the shape of the single EPR line was reproduced better by the superposition of two independent Lorentzian-derivative bands, whereas the line shape was essentially a single Lorentzian derivative at W-band and 217 GHz. Nevertheless, a single Lorentzian derivative was sufficient to achieve a reasonable accuracy in the determination of the peak-to-peak widths (10% difference at X- and Q-band compared to the sharper component in a fit with two bands) and central fields (0.2%) in all cases (see Figure 2 for a typical Q-band spectrum). The results of the analysis with one single line are reported in Table 1. At all EPR frequencies, the apparent *g*-factor was in the $g^{app} = 1.97-2.0$ region (see Figures 4 and 5). At 325 GHz, the *g*-values approached 1.9924. At X-band, the room-temperature peak-to-peak width of $[Gd(bpatcn)(H_2O)]$ was $\Delta H_{pp} \approx 210$ G and that of $[Gd(tpaen)]^-$ was $\Delta H_{pp} \approx 210$ G. Both complexes are thus slightly closer to $[Gd(dota)(H_2O)]^-$ (~90 G) than to $[Gd(dtpa)(H_2O)]^{2-}$ (~600 G). We note that, although the X-band EPR lines of $[Gd(bpatcn)(H_2O)]$ are much broader than those of [Gd(tpatcn)], some beneficial effect of the pyridinecarboxylate arms seems to be retained. In comparison, the simple polyaminocarboxylate equivalent $[Gd(nota)(H_2O)_2]$ has even broader lines, with $\Delta H_{pp} = 500$ G at room temperature.[35] At Q-band, the line width of $[Gd(tpaen)]^-$ is similar to that of $[Gd(dtpa)(H_2O)]^{2-}$ (60 G at room temperature). At higher frequencies, however, the lines become much sharper and their widths become comparable with those of $[Gd(dota)(H_2O)]^-$, whose electron spin relaxation is quite slow. The lines of $[Gd(bpatcn)(H_2O)]$ are sharper than those of $[Gd(tpaen)]^-$ at all frequencies, and sharper than those of $[Gd(dota)(H_2O)]^-$ at Q-band and above. At 217 and 325 GHz, the single line exhibited significant shoulders that can be explained by the hyperfine coupling with ^{155}Gd and ^{157}Gd, in good agreement with the results obtained for [Gd(tpatcn)],[19] as demonstrated in Figure 3.

In order to study the experimental line shape in more detail without making any assumption regarding its physical origin, we also analyzed the X-band spectra in terms of two independent overlapping bands and obtained peak-to-peak widths, central fields, and relative intensities for the two components (see Supporting Information). As noted earlier, the sharper line was very similar in width and position to the one obtained through the single-component analysis. The room-temperature peak-to-peak width of the broader component in the $[Gd(bpatcn)(H_2O)]$ spectra was $\Delta H_{pp} \approx 600$ G, and the ratio of its intensity (double

TABLE 1: Electron Spin Relaxation Parameters Obtained from the Analysis of the X-, Q- and W-band Peak-to-Peak Widths and Central Fields Using the Static + Transient ZFS Modulation Model[a]

	$[Gd(tpaen)]^-$	$[Gd(bpatcn)(H_2O)]$
$a_2/10^{10}$ s^{-1}	0.5795	0.7114
$a_{2T}/10^{10}$ s^{-1}	0.4044	0.2845
τ_R^{298}/ps	100	120
E_R/kJ mol^{-1}	15	15
τ_v^{298}/ps	3.7	2.6
E_v/kJ mol^{-1}	18.5	25.2
g	1.9924	1.9924
av rel error	0.0079	0.0206

[a] Underscored values were fixed during the least-squares adjustment.

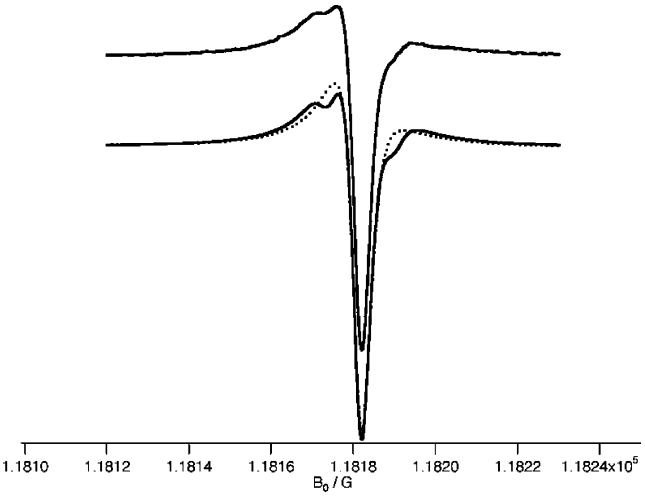

Figure 3. Experimental (upper curve) and simulated (lower curves) EPR spectra of aqueous $[Gd(bpatcn)(H_2O)]$ at 329.55 GHz and 278.7 K including (full line) and neglecting (dotted line) $^{155/157}$Gd hyperfine coupling.

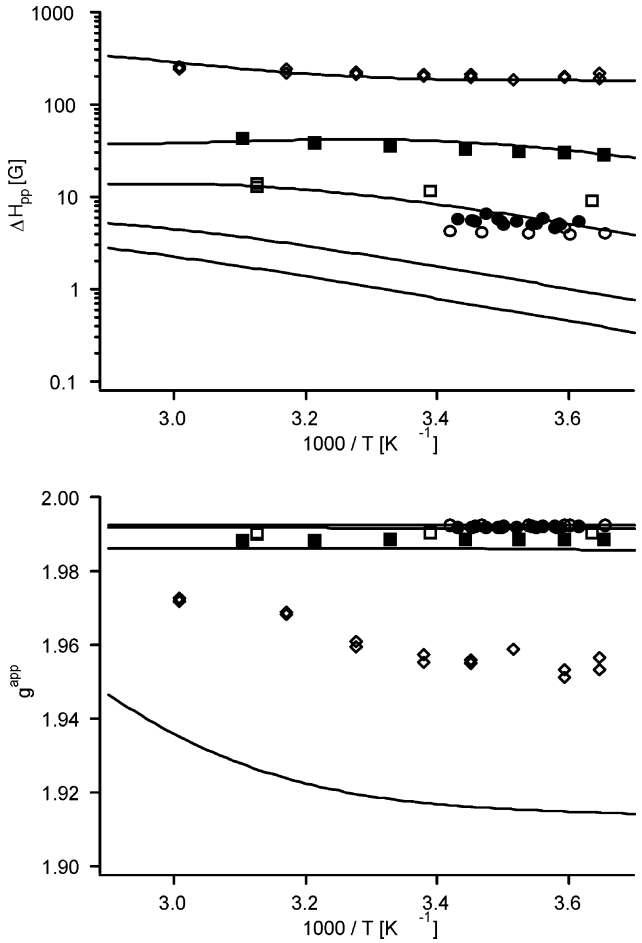

Figure 4. Experimental and theoretical peak-to-peak widths (left) and apparent g-factors for aqueous [Gd(bpatcn)(H_2O)] at X-band (◇), Q-band (■), W-band (□), 217 GHz (●), and 325 GHz (○). Theoretical curves are calculated on the basis of the fit of X-, Q-, and W-band data using the static + transient ZFS modulation model.

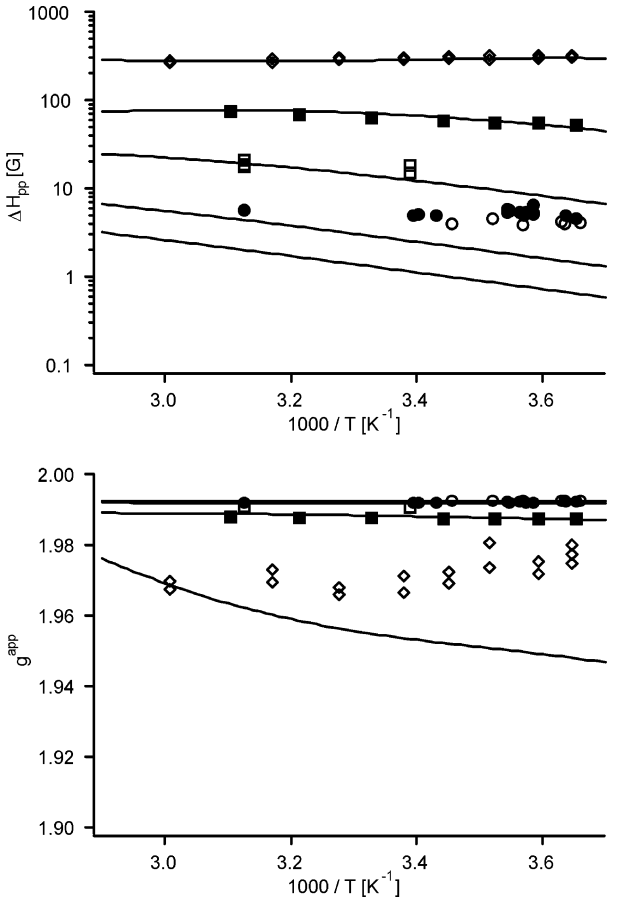

Figure 5. Experimental and theoretical peak-to-peak widths (left) and apparent *g*-factors for aqueous [Gd(tpaen)]$^-$ at X-band (◇), Q-band (■), W-band (□), 217 GHz (●), and 325 GHz (○). Theoretical curves are calculated on the basis of the fit of X-, Q-, and W-band data using the static + transient ZFS modulation model.

integral of the line with respect to the magnetic field) with respect to the sharp component was about 2.5. At Q-band, the peak-to-peak width decreased ($\Delta H_{pp} \approx 250$ G), and the intensity ratio was similar. Both the peak-to-peak width and the intensity ratio depended on temperature. The peak-to-peak widths of the broad component remain approximately the same for the [Gd(tpaen)]$^-$ samples, whereas the intensity ratio was about 1 at X-band and 2.5−4 at Q-band. One can imagine various possible causes for the non-Lorentzian shape of our spectra. However, it must be noted that the values for that broad component cannot be considered accurate. In the spectral analysis, the width and the integral of a Lorentzian band are strongly correlated (integral ≈ width × maximum height; for the derivative, the integral depends on the square of the line width). Furthermore, the integrals depend of course on the exact form of the lines. Assuming a Lorentzian derivative can induce significant systematic errors, especially when the line widths are not negligible compared to the central field, a frequent occurrence for Gd^{3+} complexes at X-band (typically, $\Delta H_{pp} =$ 100 to 1000 G depending on the complex and temperature, and $B_0 \approx 3400$ G). It is indeed generally abusive to assume that the relaxation rates (and thus the line widths) are the same throughout a continuous-wave EPR spectrum. At X-band, the Zeeman energy can change by 1 order of magnitude along the spectral window required by a typical Gd^{3+} complex. Incidentally, the latter problem also precludes a full line shape analysis using the program of Rast,[7] which uses a simple transformation from the frequency to the magnetic field dimension and would be unable to properly account for the broader component. Thus, it is very difficult to provide a quantitative analysis.

For both complexes, we could estimate the effect of concentration on the high-frequency (217 GHz and above) peak-to-peak width and found it to be around 0.1 G/mmol. Since the effect is small enough compared to the total width (always >4 G) at the concentrations used, we neglected it in our analysis and took all concentrations into account for our analysis. This is almost equivalent to a trivial increase in statistical weight of the high-frequency measurements in the fitting procedure.

The results of the analysis of the X-, Q-, and W-band EPR data using the static + transient ZFS model of Rast et al.[7,29] are shown in Table 1 and Figures 4 and 5. The peak-to-peak widths between X- and W-band were reproduced well, whereas there was a significant error in the apparent *g*-factors (i.e., central fields) for [Gd(bpatcn)(H_2O)]. Unlike for [Gd(tpatcn)], the static ZFS magnitude parameters a_2 are not small at all. This was of course expected from the X-band EPR line widths, where the static ZFS modulation process often plays a dominant role.[7,29] The low-frequency peak-to-peak widths lead to a value higher than those of [Gd(dota)(H_2O)]$^-$ and similar complexes ($a_2 =$ 0.319−0.555 × 10^{10} s^{-1}) but lower than that of [Gd(dtpa)(H_2O)]$^{2-}$ ($a_2 = 0.92 \times 10^{10}$ s^{-1}).[36] This confirms the fact that the presence of pyridine carboxylate groups in the ligand is not enough to ensure a slow electron spin relaxation. Even in the case of [Gd(tpaen)]$^-$, the fairly high nitrogen/oxygen ratio (6 vs 4) does not slow down the X-band transverse relaxation in comparison with [Gd(dota)(H_2O)]$^-$. The low symmetry (C_2 at

best) of the coordination polyhedron probably plays a negative role for $[Gd(tpaen)]^-$. The transient ZFS parameters seem to remain essentially the same for all complexes ($0.3-0.45 \times 10^{10}$ s^{-1}). This value is probably determined by the amplitude of the possible deformations of the chelate and could be optimized by designing particularly rigid ligands ($T_{1e} = 5.8$ ns at Q-band, i.e., $\omega_0 = 2.1 \times 10^{11}$ s^{-1} for $[Gd(bpatcn)(H_2O)]$ and 3.4 ns for $[Gd(tpaen)]^-$, compared to 7.7 ns for $[Gd(dota)(H_2O)]^-$ and 2.7 ns for $[Gd(dtpa)(H_2O)]^-$ using the published parameters[7,36] and the equation of Belorizky and Fries[37]). The isotropic *g*-factors of $[Gd(bpatcn)(H_2O)]$ and $[Gd(tpaen)]^-$ are almost identical to those measured for other chelates in previous studies.

It was not possible to obtain a perfect agreement between the theoretical curves and the experimental data when all EPR frequencies were taken into account. The results of the fit were significantly worse after adding the VHFEPR data than when only partial experimental data were considered, either the lower EPR frequencies or the higher ones (W-band, 217 and 325 GHz) as demonstrated by the average relative error between the experimental and simulated values (see Supporting Information). The values obtained from the analysis of the conventional EPR data yielded parameters that are unable to describe the VHFEPR line shapes. They predict peak-to-peak widths 3 to 6 times smaller at 217 and 325 GHz than what we observed experimentally. The analysis of W-band and VHFEPR data alone yielded very different parameters than those of conventional EPR or the complete data set. While the transient ZFS magnitude parameters a_{2T} of both complexes changed only slightly, the associated room-temperature correlation times τ_v^{298} were shortened down to the subpicosecond range and the static ZFS magnitude parameters a_2 increased dramatically. It has been shown that, when large enough, the latter parameter plays a dominant role at low EPR frequencies.[7,29] Thus, the simulated X-band line widths calculated from the high-frequency parameters were of course much larger than the experimental ones. They were actually in better agreement with the peak-to-peak width of the broader component estimated in a line shape analysis with two Lorentzian-derivative lines. At Q-band, the difference between the calculated peak-to-peak widths and the experimental ones decreased slightly, but the calculated lines were still twice as large as the experimental results. Overall, we observed that some numerical improvement could be achieved by including fourth- and sixth-order ZFS terms. The average difference between the experimental and calculated values decreased by a factor of 2, but the new fit was still far from perfect. Furthermore, the second-order term was close to zero in the resulting parameters, and the sixth-order term was the only significant contribution of the static ZFS to relaxation. Although a similar result was obtained recently for two gadolinium cryptate complexes in solution,[38] this finding seems physically unlikely. In the solid, high-order terms are usually much smaller[39] unless the second order vanishes because of an octahedral or higher symmetry, which is clearly not the case here.

One possible explanation for the apparent discrepancy between the low- and high-frequency measurements could be the combination of a sizable static zero-field splitting with a relatively long rotation correlation time compared with other monomeric chelates. Rast's equations, as used in this study, were developed within Redfield's theoretical framework.[40] This assumes small time-dependent Hamiltonian perturbations and rapid random modulations, which can be expressed as $a_2 \times \tau_R \ll 1$ for the second-order static ZFS modulation. According to our results, this assumption is not strictly valid for $[Gd(bpatcn)(H_2O)]$ and $[Gd(tpaen)]^-$ ($a_2 \times \tau_R^{298} = 0.85$ and 0.58, respectively).

TABLE 2: Simulated High-Frequency Peak-to-Peak Widths at Room Temperature, Using the [Gd(tpaen)] ZFS Parameters Obtained from X-, Q-, and W-band, and Increasing *g*-Tensor Anisotropy

$g_{//}$	$g_\perp$	ΔH_{pp} 217 GHz	ΔH_{pp} 325 GHz	ΔH_{pp} 500 GHz
1.9924	1.9924	2.8 G	1.3 G	0.5 G
1.994	1.992	3.9 G	3.7 G	6.4 G
1.9945	1.9915	5.3 G	6.8 G	13.6 G
exptl[a]		7.0 G	6.4 G[b]	-

[a] $T = 289.5$ K. [b] $\nu = 329.58$ GHz.

Another possible cause could be the presence of isomers in solution. This phenomenon is well-documented for $[Gd(dota)(H_2O)]^-$,[41] and one might attribute the non-Lorentzian character of the X- and Q-band lines to the superposition of several lines, due to different isomers, with different widths. Indeed, the ^1H NMR spectrum of $[Eu(bpatcn)(H_2O)]$ shows a temperature-dependent line broadening suggesting an exchange process among isomers present in solution at very different concentration.[23] However, a study of $[Eu(tpaen)]^-$ showed no such evidence.[22] Furthermore, even for the dota complex where the equilibrium between the so-called M and m isomers is well-characterized, the available EPR studies[5,7,42] never showed a clear effect of these species on the line shape. Thus, the observed line shape is more probably a consequence of the multiexponential decay of the transverse relaxation predicted by the theory. For example, by converting the four calculated transverse relaxation rates for $[Gd(bpatcn)(H_2O)]$ at room temperature into field units,[3] we observe that the second sharpest line at X- and Q-band has a peak-to-peak width compatible with our measurements for the broad component (697 and 517 G, respectively). As pointed out earlier, an accurate prediction of such broad X-band lines is a difficult problem. The combination of the Zeeman energy change along the spectrum and possible violation of the Redfield conditions means that only time-consuming spectral computations such as Monte Carlo simulations[43] or calculations involving the stochastic Liouville equation[44,45] will be able to provide a final answer to this question.

The problem of underestimated relaxation rates at high magnetic field has already been considered in the past from the point of view of EPR[5] and NMR.[42] A magnetic field independent spin-rotation mechanism[46,47] was proposed but rejected later in favor of the more reasonable static plus transient ZFS modulation process.[29] Instead, we suggest the possibility of rotational modulation of the g-tensor anisotropy. This mechanism (with an associated hyperfine tensor anisotropy) is often invoked to explain the electron spin relaxation of $S = {}^1/_2$ species, either organic radicals or transition metal ion complexes. There is some experimental evidence for such an isotropy in the solid state for Gd^{3+} doped into various diamagnetic matrices.[39] The reported anisotropies are fairly small ($0.01 > |g_{max} - g_{min}| > 0.0001$) but can provide an efficient relaxation mechanism when the external magnetic field is high enough. A straightforward application of Refield's relaxation theory, combined with Rast's work on the ZFS modulation processes, leads to the relaxation matrices presented in the Appendix. By diagonalizing the total relaxation matrix (i.e., static and transient ZFS, plus *g*-tensor anisotropy, plus cross-terms), we can predict the influence of a hypothetic *g*-tensor anisotropy on the peak-to-peak widths at very high frequencies, proportional to the slowest calculated relaxation rate ($m_S = -1/2 \rightarrow +1/2$). The results for $[Gd(tpaen)]^-$, based on the ZFS parameters obtained from X-, Q-, and W-band data, are reported in Table 2. We see

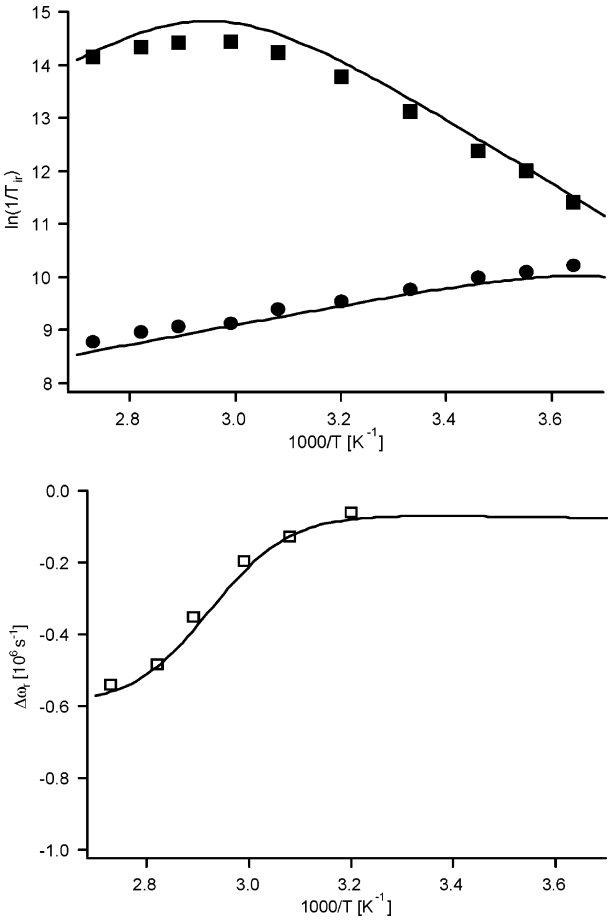

Figure 6. Experimental ^{17}O NMR relaxation for [Gd(bpatcn)(H_2O)] at 9.4 T: reduced longitudinal (●) and transverse (■) relaxation rates, chemical shifts (□). The curves were simulated using the ad hoc equations of Powell (ref 42).

that *g*-tensor anisotropy of 0.002 to 0.003 would explain the magnitude of the excess line width at 217 and 325 GHz. Furthermore, we predict an increase in the calculated peak-to-peak width at even higher frequencies as the *g*-tensor anisotropy modulation becomes the dominant relaxation process. Thus, measurements at 500 GHz (resonance field 17.93 T for $g = 1.9924$) would be the obvious way to confirm our hypothesis.

Due to the lack of a definitive answer regarding the electron spin relaxation of our chelates, we did not attempt a simultaneous analysis of EPR and NMR relaxation data. A qualitative assessment of the ^{17}O NMR relaxation rates and chemical shifts (Figure 6 and Supporting Information) is sufficient to estimate a rather slow water exchange for [Gd(bpatcn)(H_2O)]. Indeed, the maximum $1/T_{2r}$ was only observed at a fairly high temperature ($T > 345$ K), characteristic of a low k_{ex}, and the chemical shifts do not exhibit the usual plateau indicative of the fast-exchange regime at high temperature. Indeed, by analyzing the ^{17}O NMR relaxation data using the equations given by Powell,[42] we estimate $k_{ex} = 0.6 \times 10^6$ s^{-1} at 298 K, a value similar to that of the slowly exchanging complex [Gd(dtpa-bma)(H_2O)] (0.45×10^6 s^{-1}). The ^{17}O NMR data for [Gd(tpaen)]$^-$ is in agreement with the absence of any water molecule in the first coordination shell.

Conclusion

We carried out a study of two gadolinium polyamino polypyridine carboxylate complexes, [Gd(bpatcn)(H_2O)] and [Gd(tpaen)]$^-$, in aqueous solutions by EPR at multiple frequencies and ^{17}O NMR. We observe that, in comparison with other chelates studied in the recent years, their electron spin relaxation, as manifested by the EPR peak-to-peak width, is moderate at X-band and slow at higher frequencies and magnetic fields, although not as slow as for the best compounds known to date. The huge differences among the very sharp X-band EPR lines of [Gd(tpatcn)], the intermediate [Gd(bpatcn)(H_2O)] and [Gd(tpaen)]$^-$, and the broad spectrum of [Gd(bpeda)(H_2O)]$^-$ clearly show that the zero-field splitting in Gd^{3+} chelates is highly sensitive to the nature of the coordination polyhedron. [Gd(bpatcn)(H_2O)] is more suitable than [Gd(tpaen)]$^-$ as an MRI contrast agent due to the presence of one inner-sphere water molecule. However, ^{17}O NMR shows unambiguously that the water exchange is quite slow for this complex. In order to make it suitable as a building block for macromolecular compounds with a high relaxivity, the ligand framework should be modified to achieve a higher water exchange rate. At very high EPR frequencies, we find that the modern model of the electron spin relaxation of Gd^{3+} complexes, taking into account the modulation of the zero-field splitting by rotation and molecular deformations, is apparently not able to account for the observed line widths. We suggest that the rotational modulation of the *g*-tensor anisotropy might become effective under such conditions. Extrapolations suggest that the line widths of typical Gd^{3+} chelates might be reaching a minimum at 200−300 GHz and start to increase again at higher frequencies and magnetic fields. Measurements at 500 GHz/17.93 T would be a good test of this hypothesis.

Acknowledgment. We thank Dr. J. van Tol and L.-C. Brunel (NHMFL) for their assistance during the high-frequency EPR experiments, as well as for the valuable advice and discussions after the completion of the measurements. We also thank Alexander Schiller (EPFL) for the ICP-AES measurements. This work was financially supported by the Swiss National Science Foundation, the EU COST Action D18 "Lanthanide Chemistry for Diagnosis and Therapy" and the European-funded EMILE program.

Supporting Information Available: The complete EPR measurements (peak-to-peak widths and central fields, together with the equivalent apparent *g*-factor) with one and two components as a function of the temperature, spectrometer frequency, and gadolinium concentration, and the ^{17}O NMR data (longitudinal and transverse relaxation rates, chemical shifts) are available, as well as the EPR analysis results including VHFEPR. This material is available free of charge via the Internet at http://pubs.acs.org.

Appendix: Transverse Relaxation under ZFS Modulation Correlated with *g*-Tensor Anisotropy

Redfield's theory[40] can be used to predict the relaxation rates and intensities of an $S > 1/2$ spin undergoing modulation of the ZFS tensor correlated with rotational modulation of the *g*-tensor. For the sake of simplicity, we will only consider the second-order terms of the ZFS and assume that the main axis of the ZFS is the same as that of the *g*-tensor. Furthermore, we will only consider the case of an axially symmetric *g*-tensor. Finally, we will neglect the dynamic frequency shifts. This is acceptable since we are interested in the very high frequency regime, where such shifts eventually vanish.

First, we decompose the Hamiltonian responsible for relaxation into a sum of three terms, namely the so-called static ZFS

TABLE A1: Spin Tensors and Parameters for *g*-Tensor Anisotropy

q	$\hat{A}_q^2$	F_q
0	$-2\sqrt{(2/3)}\hat{S}_z$	$-\sqrt{(1/6)}(\mu_B B_0/\hbar)(g_{//} - g_\perp)$
±1	$\mp\hat{S}_\pm$	0
±2	0	0

and transient ZFS contributions,[29] plus a *g*-anisotropy modulation term.

$$\hat{H}_1^{\,L}(t) = \hat{H}_1^{\,sZFS}(t) + \hat{H}_1^{\,tZFS}(t) + \hat{H}_1^{\,g}(t) \qquad (1)$$

The explicit formulation of the time-dependent terms can be written using Wigner rotation matrices, following Rast[29] for the static and transient ZFS terms in the case of isotropic Brownian rotation. Relaxation through the modulation of *g*-anisotropy was studied in detail by Freed and Fraenkel:[48]

$$\hat{H}_1^{\,L}(t) = \sum_\eta B^{2\eta} \sum_{p,q=-2}^{+2} b_q^{k\eta} \hat{T}_q^2 D_{pq}^2(R(t)) + \sum_\eta B^{2\eta T}(t) \sum_{p,q=-2}^{+2} b_q^{2\eta T}\, \hat{T}_p^2 D_{pq}^2(R(t)) + \sum_{p,q=-2}^{+2} \hat{A}_p^2 F_q D_{pq}^2(R(t)) \quad (2)$$

We recall the explicit forms of the symbols for the *g*-tensor anisotropy term in Table A1. We can now express the elements of the Redfield relaxation matrix using the time correlation functions of the Hamiltonian matrix elements.

$$R_{\alpha\alpha'\beta\beta'} = J_{\alpha\beta\alpha'\beta'}[(\alpha' - \beta')\omega] + J_{\beta'\alpha'\beta\alpha}[(\beta - \alpha)\omega] - \delta_{\alpha'\beta'} \sum_\gamma J_{\alpha\gamma\beta\gamma}[(\beta - \gamma)\omega] - \delta_{\alpha\beta} \sum_\gamma J_{\gamma\alpha'\gamma\beta'}[(\gamma - \beta')\omega]$$

$$J_{\alpha\beta\alpha'\beta'}(\omega) = \int_0^{+\infty} \overline{\langle\alpha|H_1(t)|\beta\rangle\langle\beta'|H_1(t-\tau)|\alpha'\rangle}\, e^{-i\omega\tau}\, d\tau \qquad (3)$$

The time correlation functions are of course combinations of the three terms in the time-dependent Hamiltonian

$$\overline{\langle\alpha|H_1(t)|\beta\rangle\langle\beta'|H_1(t-\tau)|\alpha'\rangle} = \sum_{\mu,\nu=sZFS,tZFS,g} \overline{\langle\alpha|H_1^\mu(t)|\beta\rangle\langle\beta'|H_1^\nu(t-\tau)|\alpha'\rangle}$$

The self-correlation functions for the static and transient ZFS Hamiltonians lead to transverse relaxation matrices similar to those originally derived by Hudson and Lewis,[49] the relevant correlation times being the second-order rotation correlation time $\tau_R = 1/(6D_R)$ and τ', the reciprocal sum of τ_2, and the vibrational correlation time τ_v.

$$R_{2(s,t)} = \frac{1}{5} a_{(2,2T)}{}^2 \begin{pmatrix} A & E & F & 0 & 0 & 0 & 0 \\ E & B & G & H & 0 & 0 & 0 \\ F & G & C & 0 & I & 0 & 0 \\ 0 & H & 0 & D & 0 & H & 0 \\ 0 & 0 & I & 0 & C & G & F \\ 0 & 0 & 0 & H & G & B & E \\ 0 & 0 & 0 & 0 & F & E & A \end{pmatrix}$$

$$A = -(54J_0 + 174J_1 + 66J_2)$$

$$B = -(24J_0 + 174J_1 + 126J_2)$$

$$C = -(6J_0 + 784J_1 + 186J_2)$$

$$D = -(30J_0 + 210J_2)$$

$$E = 24\sqrt{21}\, J_1$$

$$F = 6\sqrt{105} J_2$$

$$G = \sqrt{120} J_1$$

$$H = 60\sqrt{3} J_2$$

$$I = 120 J_2$$

$$J_n = \frac{\tau_c}{1 + (n\omega_0\tau_c)^2}$$

$$\tau_c = \begin{cases} \text{s,static:} \tau_R \\ \text{t,transient:} \dfrac{1}{\dfrac{1}{\tau_R} + \dfrac{1}{\tau_v}} \end{cases}$$

The *g*-tensor anisotropy transverse relaxation matrix is readily calculated from the general expression of the Redfield matrix elements. Here again, the correlation time of interest is the second-order rotation correlation time τ_R.

$$R_{2g} = \left(\frac{(g_{//} - g_\perp)\mu_B B_0}{\hbar}\right)^2 \begin{pmatrix} a & e & 0 & 0 & 0 & 0 & 0 \\ e & b & f & 0 & 0 & 0 & 0 \\ 0 & f & c & g & 0 & 0 & 0 \\ 0 & 0 & g & d & g & 0 & 0 \\ 0 & 0 & 0 & g & c & f & 0 \\ 0 & 0 & 0 & 0 & f & b & e \\ 0 & 0 & 0 & 0 & 0 & e & a \end{pmatrix}$$

$$a = -\left(\frac{4}{45} J_0 + \frac{13}{15} J_1\right)$$

$$b = -\left(\frac{4}{45} J_0 + \frac{23}{15} J_1\right)$$

$$c = -\left(\frac{4}{45} J_0 + \frac{29}{15} J_1\right)$$

$$d = -\left(\frac{4}{45} J_0 + \frac{31}{15} J_1\right)$$

$$e = \frac{2}{5}\sqrt{\frac{7}{3}} J_1$$

$$f = \frac{2}{\sqrt{5}} J_1$$

$$g = \frac{4}{\sqrt{15}} J_1$$

We now address the problem of the cross-terms. Rast's development assumes independent modulation of the static and transient ZFS terms, and the same can be assumed for the transient ZFS and the *g*-tensor anisotropy. We only need to consider the cross-correlation functions of the static ZFS and *g*-tensor anisotropy Hamiltonians.

$$\overline{\langle\alpha|H_1^{sZFS}(t)|\beta\rangle\langle\beta'|H_1^{g}(t-\tau)|\alpha'\rangle} = \sum_{\eta} B^{2\eta} \sum_{p,q,p',q'=-2}^{2} b_q^{k\eta} \overline{\langle\alpha|\hat{T}_2^{p}|\beta\rangle\langle\beta'|\hat{A}_2^{p'}|\alpha'\rangle F_{q'} D_{pq}^{2}[R(t)] D_{p'q'}^{2}[R(t-\tau)]}$$

The time correlation function for the Wigner rotation matrices vanishes for Brownian rotations unless $p = p'$ and $q = q'$, and we can write

$$\overline{\langle\alpha|H_1^{sZFS}(t)|\beta\rangle\langle\beta'|H_1^{g}(t-\tau)|\alpha'\rangle} = \sum_{\eta} B^{2\eta} \sum_{p,q=-2}^{2} b_q^{k\eta} \langle\alpha|\hat{T}_2^{p}|\beta\rangle \langle\beta'|\hat{A}_2^{p}|\alpha'\rangle F_q \times \frac{1}{5}\exp\left(-\frac{\tau}{\tau_2}\right)$$

The other, and last, cross-term is of course

$$\overline{\langle\alpha|H_1^{g}|\beta\rangle\langle\beta'|H_1^{sZFS}(t)(t-\tau)|\alpha'\rangle} = \sum_{\eta} B^{2\eta} \sum_{p,q=-2}^{2} b_q^{k\eta} \langle\alpha|\hat{A}_2^{p}|\beta\rangle \langle\beta'|\hat{T}_2^{p}|\alpha'\rangle F_q \times \frac{1}{5}\exp\left(-\frac{\tau}{\tau_2}\right)$$

With these expressions, we can now construct the cross-correlation matrix elements and the total transverse relaxation matrix R_2. In our case, all terms containing the rhombic ZFS coefficient $B^{20} = 2^{1/2}E_{ZFS}$ vanish in the summation. By remembering that $B^{20} = (2/3)^{1/2}D_{ZFS}$,[50] we can write

$$R_{2x} = \left(\frac{2(g_{//} - g_{\perp})\mu_B B_0}{\hbar}\right) D_{ZFS} J_0 \begin{pmatrix} -\frac{4}{5} & 0 & 0 & 0 & 0 & 0 & 0 \\ 0 & -\frac{8}{15} & 0 & 0 & 0 & 0 & 0 \\ 0 & 0 & -\frac{4}{15} & 0 & 0 & 0 & 0 \\ 0 & 0 & 0 & 0 & 0 & 0 & 0 \\ 0 & 0 & 0 & 0 & \frac{4}{15} & 0 & 0 \\ 0 & 0 & 0 & 0 & 0 & \frac{8}{15} & 0 \\ 0 & 0 & 0 & 0 & 0 & 0 & \frac{4}{5} \end{pmatrix}$$

We see that, since this cross-correlation term R_{2x} is not influenced by the rhombic ZFS, it is not possible to obtain it directly from the magnitude term a_2. Furthermore, we note that the sign of D_{ZFS}, which plays no role in the pure ZFS relaxation mechanism (a_2 is positive by definition and always appears squared), directly affects the sign of R_{2x}. The same is of course true for the g-tensor anisotropy.

The final relaxation matrix is trivially given by

$$R_2 = R_{2s} + R_{2t} + R_{2g} + R_{2x}$$

The eigenvalues and eigenvectors of the relaxation matrix yield the relaxation rates and intensities, respectively. At very high frequencies, the EPR spectrum is dominated by the $-1/2 \rightarrow +1/2$ transition, which corresponds to the slowest transition (i.e., the sharpest line).

References and Notes

(1) Caravan, P.; Ellison, J. J.; McMurry, T. J.; Lauffer, R. B. *Chem. Rev.* **1999**, *99*, 2293.

(2) Merbach, A. E.; Tóth, É. *The Chemistry of Contrast Agents in Medical Magnetic Resonance Imaging*; John Wiley & Sons, Ltd.: Chichester, U.K., 2001.

(3) Powell, D. H.; Merbach, A. E.; Gonzalez, G.; Brücher, E.; Micskei, K.; Ottaviani, M. F.; Köhler, K.; von Zelewsky, A.; Grinberg, O. Y.; Lebedev, Y. S. *Helv. Chim. Acta* **1993**, *76*, 2129.

(4) Sur, S. K.; Bryant, R. G. *J. Phys. Chem.* **1995**, *99*, 6301.

(5) Clarkson, R. B.; Smirnov, A. I.; Smirnova, T. I.; Kang, H.; Belford, R. L.; Earle, K.; Freed, J. H. *Mol. Phys.* **1998**, *95*, 1325.

(6) Borel, A.; Tóth, É.; Helm, L.; Jánossy, A.; Merbach, A. E. *Phys. Chem. Chem. Phys.* **2000**, *2*, 1311.

(7) Rast, S.; Borel, A.; Helm, L.; Belorizky, E.; Fries, P. H.; Merbach, A. E. *J. Am. Chem. Soc.* **2001**, *123*, 2637.

(8) Tóth, É.; Pubanz, D.; Vauthey, S.; Helm, L.; Merbach, A. E. *Chem.—Eur. J.* **1996**, *2*, 1607.

(9) Dunand, F. A.; Toth, E.; Hollister, R.; Merbach, A. E. *J. Biol. Inorg. Chem.* **2001**, *6*, 247.

(10) Nicolle, G. M.; Toth, E.; Eisenwiener, K. P.; Macke, H. R.; Merbach, A. E. *J. Biol. Inorg. Chem.* **2002**, *7*, 757.

(11) Nicolle, G. M.; Toth, E.; Schmitt-Willich, H.; Raduchel, B.; Merbach, A. E. *Chem.—Eur. J.* **2002**, *8*, 1040.

(12) Nicolle, G. M.; Tóth, É.; Eisenwiener, K.-P.; Mäcke, H. R.; Merbach, A. E. *J. Biol. Inorg. Chem.* **2002**, *7*, 757.

(13) Caravan, P.; Cloutier, N. J.; Greenfield, M. T.; McDermid, S. A.; Dunham, S. U.; Bulte, J. W. M.; Amedio, J. C.; Looby, R. J.; Supkowski, R. M.; Horrocks, W. D.; McMurry, T. J.; Lauffer, R. B. *J. Am. Chem. Soc.* **2002**, *124*, 3152.

(14) Caravan, P.; Greenfield, M. T.; Li, X. D.; Sherry, A. D. *Inorg. Chem.* **2001**, *40*, 6580.

(15) Aime, S.; Barge, A.; Borel, A.; Botta, M.; Chemerisov, S.; Merbach, A. E.; Müller, U.; Pubanz, D. *Inorg. Chem.* **1997**, *36*, 5104.

(16) Bretonniere, Y.; Mazzanti, M.; Pecaut, J.; Dunand, F. A.; Merbach, A. E. *Inorg. Chem.* **2001**, *40*, 6737.

(17) Bretonniere, Y.; Mazzanti, M.; Pecaut, J.; Dunand, F. A.; Merbach, A. E. *Chem. Commun.* **2001**, 621.

(18) Gateau, C.; Mazzanti, M.; Pécaut, J.; Dunand, F. A.; Merbach, A. E. *J. Chem. Soc., Dalton Trans.* **2003**, *12*, 2428.

(19) Borel, A.; Kang, H.; Gateau, C.; Mazzanti, M.; Clarkson, R. B.; Belford, R. L. *J. Phys. Chem. A* **2006**, *110*, 12434.

(20) Fries, P. H.; Gateau, C.; Mazzanti, M. *J. Am. Chem. Soc.* **2005**, *127*, 15801.

(21) Chatterton, N.; Gateau, C.; Mazzanti, M.; Pécaut, J.; Borel, A.; Helm, L.; Merbach, A. E. *Dalton Trans.* **2005**, 1129

(22) Chatterton, N.; Bretonnière, Y.; Pécaut, J.; Mazzanti, M. *Angew. Chem., Int. Ed.* **2005**, *44*, 7595.

(23) Nonat, A.; Gateau, C.; Fries, P. H.; Mazzanti, M. *Chem.—Eur. J.* **2006**, *12*, 7133.

(24) Amman, C.; Meier, P.; Merbach, A. E. *J. Magn. Reson.* **1982**, *46*, 319.

(25) Schmalbein, D.; Maresch, G. G.; Kamlovski, A.; Hofer, P. *Appl. Magn. Reson.* **1999**, *16*, 185.

(26) Smith, G. M.; Lesurf, J. C. G.; Mitchell, R. H.; Riedi, P. C. *Rev. Sci. Instrum.* **1998**, *69*, 3924.

(27) Helm, L.; Borel, A. *NMRICMA*, 2.7 ed.; ICMA: Lausanne, 2000.

(28) Rast, S.; Fries, P. H.; Belorizky, E. *J. Chim. Phys.* **1999**, *96*, 1543.

(29) Rast, S.; Fries, P. H.; Belorizky, E. *J. Chem. Phys.* **2000**, *113*, 8724.

(30) Connolly, M. L. *J. Appl. Crystallogr.* **1983**, *16*, 548.

(31) Brunisholz, G.; Randin, M. *Helv. Chim. Acta* **1959**, *42*, 1927.

(32) Hugi, A. D.; Helm, L.; Merbach, A. E. *Helv. Chim. Acta* **1985**, *68*, 508.

(33) Vold, R. L.; Waugh, J. S.; Klein, M. P.; Phelps, D. E. *J. Chem. Phys.* **1968**, *48*, 3831.

(34) Meiboom, S.; Gill, D. *Rev. Sci. Instrum.* **1958**, *29*, 688.

(35) Geraldes, C. F. G. C.; Brown, R. D., III; Brucher, E.; Koenig, S. H.; Sherry, A. D.; Spiller, M. *Magn. Reson. Med.* **1992**, *27*, 284.

(36) Borel, A.; Helm, L.; Merbach, A. E.; Atsarksin, V. A.; Demidov, V. V.; Odintsov, B. M.; Belford, R. L.; Clarkson, R. B. *J. Phys. Chem. A* **2002**, *106*, 6229.

(37) Belorizky, E.; Fries, P. H. *Phys. Chem. Chem. Phys.* **2004**, *6*, 2341.

(38) Benmelouka, M.; Borel, A.; Moriggi, L.; Helm, L.; Merbach, E. *J. Phys. Chem. B* **2007**, *111*, 832.

(39) Misra, S. K. Transition Ion Data Tabulation: Gd3+ 4f7. In *Handbook of Electron Spin Resonance*; Poole, C. P. J., Farach, H. A., Eds.; Springer: New York, 1999; Vol. 2, p 257.

(40) Redfield, A. G. The Theory of Relaxation Processes. In *Advances in Magnetic Resonance*; Waugh, J. S., Ed.; Academic Press Inc.: New York, 1965; Vol. 1, p 1.

(41) Aime, S.; Barge, A.; Benetello, F.; Bombierei, G.; Botta, M.; Uggeri, F. *Inorg. Chem.* **1997**, *36*, 3287.

(42) Powell, D. H.; Ni Dubhghaill, O. M.; Pubanz, D.; Helm, L.; Lebedev, Y. S.; Schlaepfer, W.; Merbach, A. E. *J. Am. Chem. Soc.* **1996**, *118*, 9333.

(43) Rast, S.; Fries, P. H.; Belorizky, E.; Borel, A.; Helm, L.; Merbach, A. E. *J. Chem. Phys.* **2001**, *115*, 7554.
(44) Zhou, X.; Westlund, P.-O. *Spectrochim. Acta, Part A* **2005**, *62*, 335.
(45) Borel, A.; Clarkson, R. B.; Belford, R. L. *J. Chem. Phys.* **2007**, *126*, 054510/1.
(46) Curl, R. F. J. *Mol. Phys.* **1965**, *9*, 585.
(47) Nyberg, G. *Mol. Phys.* **1967**, *12*, 69.
(48) Freed, J. H.; Fraenkel, G. K. *J. Chem. Phys.* **1963**, *39*, 326.
(49) Hudson, A.; Lewis, J. W. E. *Trans. Faraday Soc.* **1970**, *66*, 1297.
(50) Borel, A.; Helm, L.; Merbach, A. E. Molecular Dynamics of Gd-(III) Complexes in Aqueous Solution by HF EPR. In *Very High Frequency (VHF) ESR/EPR*; Grinberg, O. Y., Berliner, L. J., Eds.; Kluwer: New York, 2004; p 207.